Introduction: Loading of a residual limb within a prosthetic socket can cause tissue damage such as ulceration. Computational models and simulations may be useful tools for estimating tissue loading within the socket and thus provide insights into how interventions (e.g. prosthesis designs or rehabilitation techniques) affect residual limb-socket interface dynamics. The purpose of this study was to model and simulate residual limb-socket interface dynamics and evaluate the effects of varied prosthesis stiffness on interface dynamics during gait. **Methods**: A spatial contact model of a residual limb-socket interface was developed and integrated into a gait model with a below-knee amputation. Gait trials were simulated for four subjects walking with low, medium, and high prosthesis stiffness settings. The effects of prosthesis stiffness on interface kinematics, normal pressure, and shear stresses were evaluated. Mean group responses and a subject-specific case study were analyzed. **Results**: Model-predicted outcome values were similar to those reported previously in sensor-based experiments; however, there were no discernable effects of prosthesis stiffness on interface dynamics among the group data ($p>0.05$). Subject-specific data showed decreased external rotation in the low stiffness trials, though high variability was present in the data. **Conclusions**: These methods may be useful to aid experimental studies by providing insights into the effects of varied prosthesis design parameters or gait conditions on residual limb-socket interface dynamics. Data suggest that these effects may be subject-specific.

1. Introduction

Rehabilitation following a lower limb amputation (LLA) often includes prescription of a prosthesis designed to replace the functionality of the removed limb. For an individual with a below-knee amputation (BKA), a prosthesis system typically consists of a socket, which interfaces with the residual limb, a rigid pylon, and a foot-ankle prosthesis. Use of lower limb prostheses can improve mobility, health, and quality of life. However, abnormal loading of the soft tissues surrounding the truncated shank (e.g. asymmetric pressure distribution and elevated shear forces) can cause tissue deformation and ischemia during load bearing activities (Portnoy et al., 2009). These conditions can lead to cell death, macerate tissue, and give rise to ulceration and pain (J. T. Highsmith & Highsmith, 2007).

Dermatological issues are experienced by 75% of individuals using lower limb prostheses (J. T. Highsmith & Highsmith, 2007; M. J. Highsmith et al., 2016), at 65% greater incidence compared to their counterparts with intact limbs (M. J. Highsmith et al., 2016). These conditions lead to prosthesis disuse (Meulenbelt, Dijkstra, Jonkman, & Geertzen, 2006) and can cause an individual with BKA to become wheelchair-bound. Recent estimates suggest that 11-22% of individuals abandon their prosthesis within one year of prescription (Balk et al., 2018). These data are supported by a second report which found that 25% of users abandoned prosthetic limbs, with 29% citing discomfort, 25% citing pain, and 12% claiming poor fit as the determining factor (*National Health Services Audit Commission Briefing: Assisting Independence*, 2002). This transition represents a substantial reduction in quality of life and increased healthcare-related financial burden.

The socket is a crucial component of mobility and quality of life for individuals with BKA due to its role as the interface between the human, prosthesis system, and gait environment. An improved understanding of biomechanical interaction between the residual limb and prosthetic socket during gait is necessary to attenuate rates of tissue damage and prosthesis disuse. Previous experiments evaluating residual limb-socket interface dynamics have relied on sensors integrated into the prosthetic socket (Al-Fakih, Osman, Eshraghi, & Adikan, 2013; Courtney, Orendurff, & Buis, 2016; Laszczak, Jiang, Bader, Moser, & Zahedi, 2015; Laszczak et al., 2016; Joan E. Sanders & Daly, 1993; Schiff et al., 2014). However, previous systems have utilized bulky sensors (Al-Fakih et al., 2013; Laszczak et al., 2015, 2016), tethered cables (Ali et al., 2013; Boutwell, Stine, Hansen, Tucker, & Gard, 2012; Courtney et al., 2016; Gholizadeh et al., 2014; Laszczak et al., 2015, 2016; Safari, Tafti, & Aminian, 2015; Schiff et al., 2014), or required modifications to the socket (Al-Fakih et al., 2013; Schiff et al., 2014), thereby compromising the integrity of the socket interface and likely altering gait mechanics of participants.

Simulations based on computational models may be useful for evaluating the relationships between anatomical morphologies, gait mechanics, design of prosthesis systems, and residual limb loading conditions. Previous model-based research has primarily employed finite element (FE) analysis techniques to derive dynamic mathematical models of the residual limb-socket interface (Jia, Zhang, & Lee, 2004; Lee, Zhang, Jia, & Cheung, 2004; Portnoy et al., 2009; Schiff et al., 2014). While FE models allow for complex characterization of the biological materials and their mechanical properties, they are computationally costly and thus may be limiting factors when integrated within complex gait models. Other studies have used abstract representations of the interface, such an idealized joint parameterized with spring and damper force laws (LaPrè, Price, Wedge, Umberger, & Sup, 2018). These methods may be appropriate for estimating generalized residual limb kinematics within the socket, but are unable to differentiate the forces and torques applied (e.g. normal pressure and shear stresses) and offer little insight regarding the relative load distribution at different anatomical locations around the limb. There remains a need for a computationally economical reduced order model of the biomechanical contact forces arising from the residual limb-socket interaction during gait.

This paper presents the design and development of a spatial contact force model motivated by the material properties of the residual limb and prosthetic socket. The contact model was integrated into a larger computational gait model in order to simulate kinematics and kinetics at the socket interface during gait. This model could assist experimental studies by providing insight into the effects of varied prosthesis design parameters or gait conditions on residual limb-socket interface dynamics.

2. Methods

2.1 Model Design

A spatial contact model of the residual limb-socket interface was developed in Simscape Multibody (Mathworks Inc, Natick, MA). The geometry of the residual limb bone element was simplified as a rectangular cuboid with struts to represent the dimensions of the limb inclusive of the soft tissue (Figure 1). Within the residual limb model, soft tissue and bone element mechanics are not differentiated

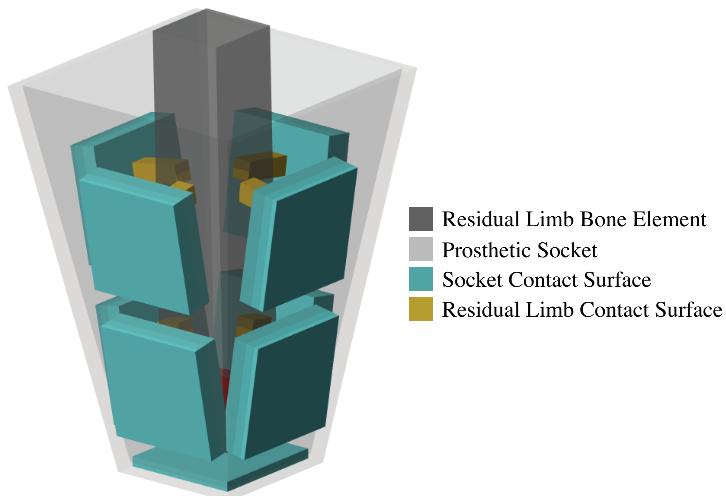

Figure 1: Depiction of the rotationally symmetrical residual limb and socket geometries, as well as the nine interface frames.

(i.e. the modeled dynamics are considered to be an aggregate of soft tissue and bone mechanics). The prosthetic socket was modeled as a rigid hollow square cone with an aperture of 100 deg. The residual limb interfaces with the socket at the same angle. The residual limb and socket have nine interface frames with attached cuboid structures to model interface dynamics. The mass of the residual limb was estimated first by deriving estimated density of the intact limb by modeling it as a conical frustum with an assigned mass estimated per De Leva (1996). The derived density of the intact limb was applied to the residual limb model, which was then truncated at the respective level of amputation for each subject. The mass of the residual limb was distributed evenly as point masses about the nine interface frames. The residual limb has two contact interfaces (one proximal, one distal) on each of the four sides of the cuboid. The ninth interface is between the distal limb and base of the prosthetic socket. The distance between the distal residual limb and base of the socket was assumed to be 1.5 cm (Henrikson et al., 2018). This distance is representative of an air gap, which is common between the socket and liner in prosthetic socket systems (Henrikson et al., 2018). Figure 1 depicts a rotationally symmetrical rendering of the model.

Contact forces at the interfaces between the limb and socket in the normal plane are implemented as modified Kelvin-Voigt material models with progressive spring and damper characteristics. Shear stresses between the socket and residual limb are considered analogous to the frictional forces arising from these interactions. In total, the residual limb has 4 degrees of freedom (DoF) with respect to the prosthetic socket (vertical translation (i.e. pistoning) and rotations about three axes).

2.2 Model Parameterization

A Kelvin-Voigt material model (spring and damper force law) was implemented to estimate residual limb-prosthetic socket interaction forces. The model estimates normal (F_n) and frictional forces (F_f) associated with the collision between a viscoelastic residual limb (spring and damper system) and rigid prosthetic socket (eq. 1). The present model does not include a socket-liner interface, but one could be implemented in the future. The spring force (k) increases as a function of penetration depth (δ), whereas damping force (b) increases with penetration velocity ($\dot{\delta}$). Damping force is only applied when $\dot{\delta} > 0$. Frictional forces are calculated as the product of normal force and a user-defined coefficient of friction

$$\textbf{eq. 1: } F_n = \begin{cases} (k * \delta) + (b * \dot{\delta}) & \delta > 0, \dot{\delta} > 0 \\ k * \delta & \delta > 0, \dot{\delta} < 0 \\ 0 & \delta < 0 \end{cases}$$

$\boldsymbol{F_n}$: normal force
$\boldsymbol{k}$: contact stiffness
$\boldsymbol{\delta}$: penetration depth
$\boldsymbol{b}$: contact damping coefficient

(μ) (eq. 2). A stick-slip friction law defines the transition between static (μ_{static}) and kinetic ($\mu_{kinetic}$) coefficients of friction based on a velocity threshold (v_{thresh}). Forces are applied along a common contact plane and conform to Newton's Third Law of Motion.

$$\textbf{eq. 2: } F_f = \begin{cases} F_n * \mu_{static} & v_{poc} < v_{threshold} \\ F_n * \mu_{kinetic} & v_{poc} > v_{threshold} \end{cases}$$

$\boldsymbol{F_f}$: frictional force
$\boldsymbol{\mu}$: coefficient of friction
$\boldsymbol{v_{poc}}$: velocity at point of contact
$\boldsymbol{v_{threshold}}$: velocity threshold

Values for spring stiffness in the normal plane (k_n) were formulated according to Hooke's Law (eq. 3), as described in Noll et al. (2017) and Zheng et al. (1999). The effective tissue moduli for individuals with a below-knee LLA (Table 1) were previously described in Zheng et al. (1999) and

$$\textbf{eq. 3: } k_n = \frac{EA}{l}$$

$\boldsymbol{k_n}$: Stiffness in the normal plane
$\boldsymbol{E}$: Young's modulus of the tissue
$\boldsymbol{A}$: Area of the contact point
$\boldsymbol{l}$: Width of the residual limb

Mak et al. (1994). In both studies, Poisson's ratio was assumed to be 0.45. The stiffness values were parameterized independently for the anterior, posterior, medial, lateral, and distal contact interfaces in order to best represent the varying moduli at corresponding anatomical locations. Due to a lack of information reported in previous literature, damping coefficients (N·s/mm) were set to half the numerical value of stiffness (N/mm) in an effort to reduce high frequency oscillations at the contact interfaces, which can lead to rapidly-evolving ordinary differential equations and thus computational instability when simulating interface dynamics.

Table 1: Summary of Young's Modulus values for various anatomical locations on the residual limb.

Anatomical location	**Effective modulus (kPa)**	**Corresponding interface(s) on the model**
Tibial tuberosity[1]	105	Anterior
Posterior tibia[3]	30	Posterior
Distal tibia[1]	60	Distal
Medial proximal tibia[2]	56	Medial

Lateral proximal tibia[1]	78	Lateral

[1](Zheng et al., 1999)
[2](Mak et al., 1994)
[3](Shan et al., 2019)

The static coefficient of friction (μ_{static}) between the limb and socket was assigned a value of 0.5, based on an *in vivo* study of the interaction between silicon (a commonly used material for prosthetic socket liners) and the skin of the human leg (Zhang and Mak, 1999). Coefficients of friction between 0.5 and 3.0 have been reported for various other socket liner materials (Cagle, Hafner, Taflin, & Sanders, 2018; Joan E Sanders, Greve, Mitchell, & Zachariah, 1998). The dynamic coefficient of friction ($\mu_{dynamic}$) was set to 70% of the μ_{static} based on Cagle et al. (2018). A velocity threshold (μ_{vth}) of 0.005 m/s defines the transition between the two values. In the future, subject-specific values for μ_{static} and $\mu_{dynamic}$ could be implemented.

The developed model predicts normal pressure and shear stress at the contact interfaces. Based on these forces, relative kinematics between the residual limb and prosthetic socket are simulated. Model-derived estimates may be compared to the range of experimental values reported in the literature for pressure, shear stress, and residual limb kinematics (Courtney et al., 2016; Eshraghi, Osman, Gholizadeh, Karimi, & Ali, 2012; Gholizadeh et al., 2014; Jia et al., 2004; LaPrè et al., 2018; Laszczak et al., 2016; J E Sanders, Zachariah, Baker, Greve, & Clinton, 2000; Joan E. Sanders & Daly, 1993). Previously-reported peak values for normal pressure range from 40-160 kPa (Ali et al., 2013; Courtney et al., 2016; J E Sanders et al., 2000), and peak values for shear stress range from 3-50 kPa (Laszczak et al., 2016; Noll et al., 2017; Sanders and Daly, 1993; Schiff et al., 2014). The broad range of values in the literature may be attributed to variation in sensors used, sensor placement, socket materials, individual-specific residual limb tissue properties, and experimental gait protocols. Further, values should vary based on phase of the gait cycle and anatomical location (Courtney et al., 2016; Noll et al., 2017; Portnoy et al., 2009; Joan E. Sanders & Daly, 1993). Nevertheless, values within these ranges may be used as target criteria.

The reported values for kinematics between the residual limb and prosthetic socket also vary within the literature. Values of 1.0 to 4.2 cm have been reported for relative vertical translation (i.e. residual limb pistoning) (Eshraghi et al., 2012; Gholizadeh et al., 2011; LaPrè et al., 2018; Joan E. Sanders, Karchin, Fergason, & Sorenson, 2006). These values may vary based on residual limb shape (Wirta, Golbranson, Mason, & Calvo, 1990) and type of socket liner used (Eshraghi et al., 2012; Gholizadeh et al., 2011; Joan E. Sanders et al., 2006). Reported values for axial internal/external rotation (rotation about the residual limb's long axis) are between 0 and ±20 deg during gait (LaPrè et al., 2018). The spatiotemporal patterns and magnitude of rotation demonstrated high variability across subjects.

2.3 Gait Simulations

The spatial contact model of the residual limb-socket interface was integrated into a gait model with a BKA and a semi-active variable stiffness foot (VSF) prosthesis. This model was previously described in McGeehan et al. (2021a and 2021b). As in McGeehan et al. (2021b), gait simulations were

Table 2: Participant characteristics.

Subject	Sex	Age (y)	Height (cm)	Mass (kg)	Amputation side	Years post-amputation
1	Male	34	181	77.3	Right	15
2	Male	51	175	111	Right	8
3	Male	70	180	83.8	Left	14
4	Female	61	163	63.8	Right	8
Mean ± SD	–	54 ± 15	175 ± 19.9	84.0 ± 19.9	–	11 ± 3.8

computed for four individuals (Table 2) walking with the VSF configured to "high", "medium", and "low" stiffness settings, corresponding to forefoot stiffness values of 10, 19, and 32 N/mm. Forward kinematics simulations were computed for three trials per setting. Subject 2 did not complete one medium stiffness trial, and Subject 4 did not complete one high stiffness trial. In total, 34 simulations were computed. All simulations were computed in Simscape Multibody using the *ode23t* solver profile with variable step sizes for numerical integration. Simulations were performed on a computer with a 4.0 GHz quad-core processor.

The experimental motion capture data used to drive the model were insufficient to estimate kinematics of the residual limb with respect to the prosthetic socket. As such, data from the literature were used to constrain motion of the residual limb via a bearing joint. A progressive spring and damper force law was used to constrain motion. Limits of 0.5 cm and -3.5 cm were imposed for residual limb vertical translation (Darter, Sinitski, & Wilken, 2016; Eshraghi et al., 2012; Gholizadeh et al., 2011; LaPrè et al., 2018; Joan E. Sanders et al., 2006). Constraints of ±10 deg, ±5 deg, and ±5 deg were imposed for axial rotation, anterior-posterior, and medial-lateral rotations (LaPrè et al., 2018; Laprè, Umberger, & Sup, 2014).

Normal forces, frictional forces, pistoning displacement, and axial rotations were estimated using the spatial contact model for the duration of stance phase. All kinematic and kinetic signals related to the limb-socket interface were low-pass filtered via a 4^{th} order Butterworth (f_c: 6Hz). Data were indexed from heel strike to toe-off and resampled to 101 data points via cubic spline interpolation. These methods allow for comparison of stance phases of different lengths. Model-derived values were compared to those previously reported in the literature. The effects of prosthesis stiffness on these outcomes were also evaluated via repeated measures ANOVA analyses ($\alpha = 0.05$). It was hypothesized that these effects would be subject-dependent, and as such, an exemplary case study for Subject 1 is presented along with group mean data.

3.0 Results

3.1 Model Performance (Group Data)

Contact model-derived values for normal pressure and shear stress were dependent upon anatomical location (Table 3) and progression of stance phase (Figure 2). Peak average normal pressure across stance phase was 70.4 ± 4.28, 75.9 ± 4.44, and 85.0 ± 13.0 kPa for the low, medium, and high stiffness conditions, whereas peak average shear stress values were 25.0 ± 1.52, 26.6 ±1.55, and 29.9 ± 4.61 kPa for the same conditions (Table 5, Figure 2). There was no main effect of stiffness condition on normal pressure ($p = 0.28$) nor shear stress ($p = 0.31$). Similar values for average residual limb pistoning and axial rotation were observed for each of the stiffness conditions ($p > 0.05$) (Figure 2), though effects were subject-dependent (Table 3). Average peak pistoning values were 1.46 ± 0.03, 1.52 ± 0.05, and 1.51 ± 0.07 cm for the ascending stiffness conditions.

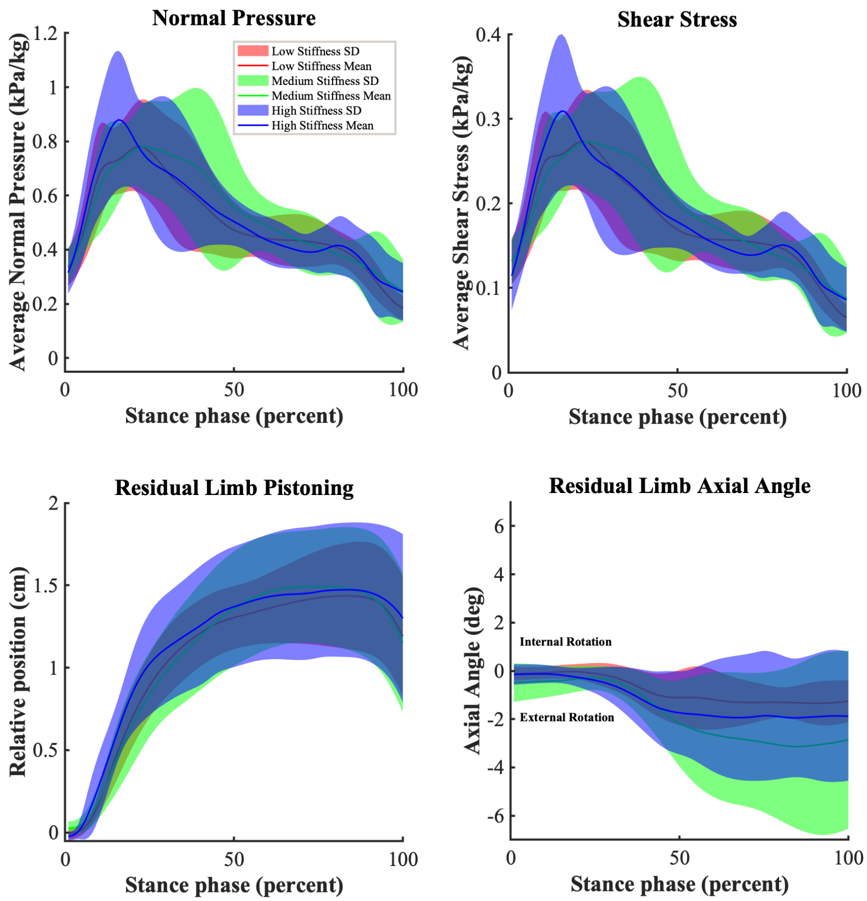

Figure 2: Group mean data for normal pressure, shear stress, residual limb pistoning, and residual limb internal/external rotation across stance phase for the low, medium, and high stiffness conditions. Kinetic data are normalized to subject body weight.

Spatiotemporal patterns for pressure and shear stress distribution were variable between subjects, but show similar variability across stiffness conditions (Tables 4 and 5, Figure 3). On average, participants displayed predominantly anterior pressure and shear distributions early in stance phase, but trended toward a more even distribution later in stance phase. Pressure trended slightly toward the lateral and proximal aspects of the residual limb thoughout stance phase. High variability was observed among participants for the anterior-posterior and medial-lateral distributions throughout stance phase.

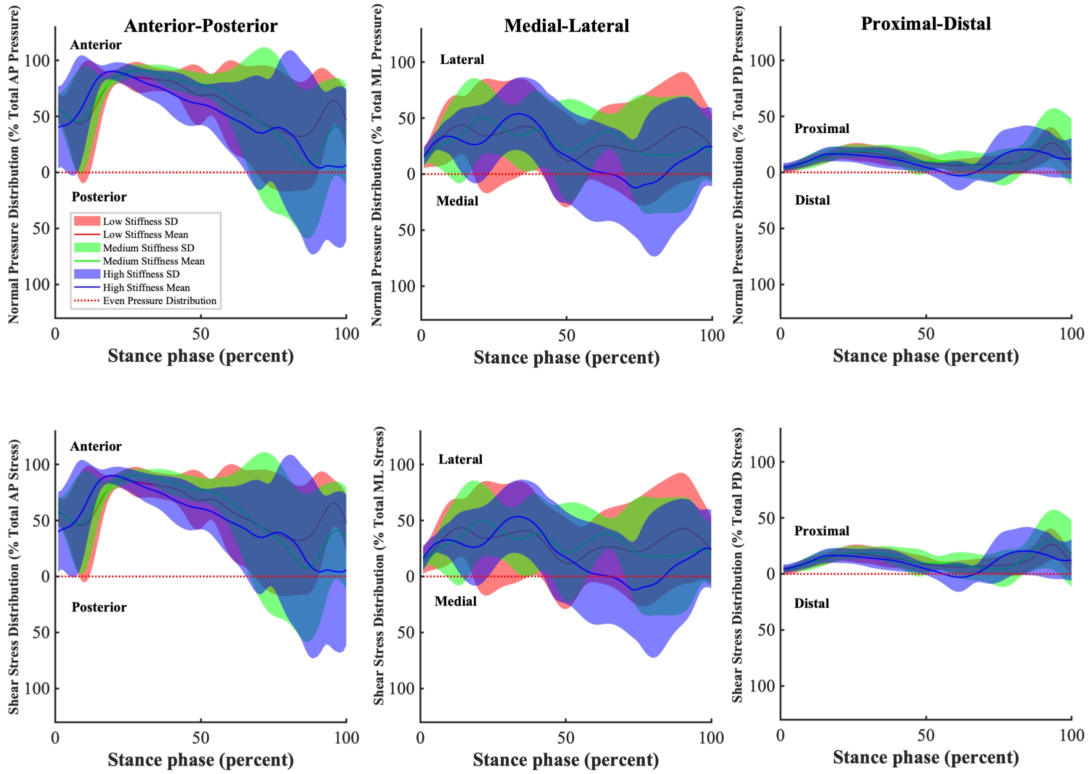

Figure 3: Group mean data for normal pressure (top) and shear stress (bottom) distributions in the anterior-posterior, medial-lateral, and proximal-distal directions.

3.1 Case Study (Subject 1)

Mean data for Subject 1 demonstrated less variability compared to the group data (Figure 4). Average pressure and shear stress values peaked at approximately 20% stance phase, whereas residual limb pistoning peaked and plateaued near 50% stance phase. Maximal pistoning displacement was approximately 1.5 cm for all conditions. A slightly increased rate of pistoning was observed between 15-40% stance phase for the high stiffness compared to the low and medium stiffness conditions (Figure 4). The subject's residual limb was predominately externally rotated with respect the prosthetic socket throughout stance phase with maximal external rotation occurring near 50% stance phase (Figure 4). The low stiffness condition resulted in the least external rotation, though high variability was observed late in stance phase for all conditions.

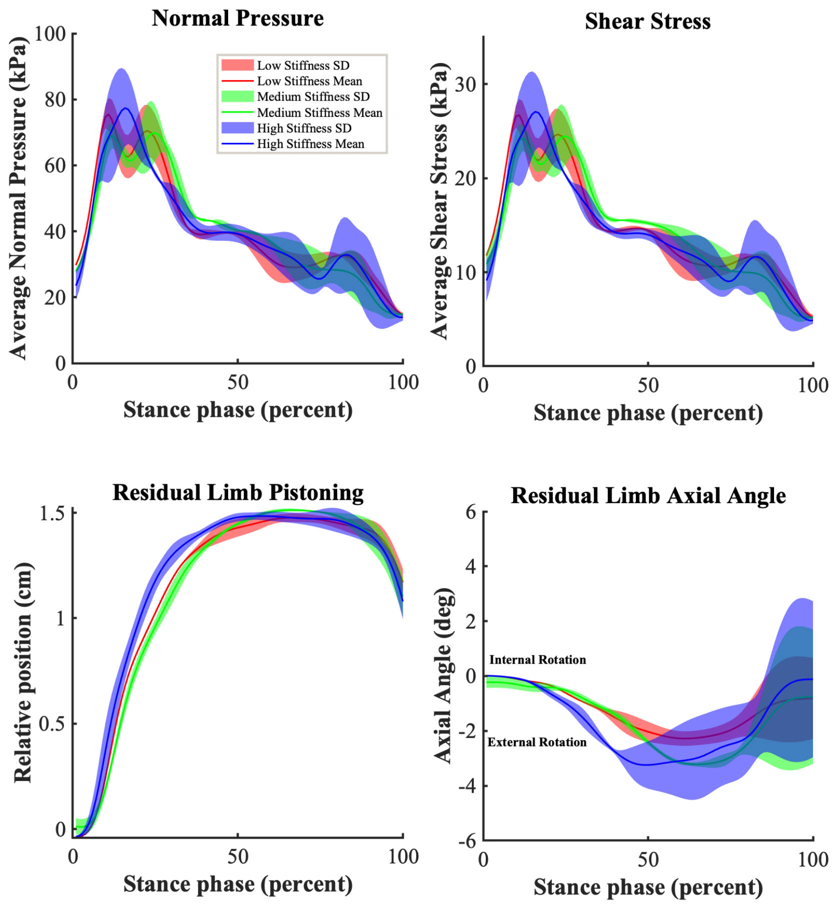

Figure 4: Mean data for normal pressure, shear stress, residual limb pistoning, and residual limb internal/external rotation across stance phase for the low, medium, and high stiffness conditions. Kinetic data are normalized to subject body weight.

The effects of variable prosthesis stiffness on pressure and shear stress distribution were observed primarily during 50-100% of stance phase (Figure 5). However, divergent patterns in the mean data were accompanied by greater variability during this time. From 0-50% stance phase, pressure and shear stress were weighted more heavily toward the anterior aspect of the residual limb for all stiffness conditions. For the low and high stiffness conditions, mean pressure and shear stress trended toward a relatively even anterior-posterior distribution late in stance phase, whereas the medium stiffness condition resulted in a relatively posterior distribution. Pressure and shear stress distribution outcomes were similar across stiffness conditions for the medial-lateral and proximal-distal directions.

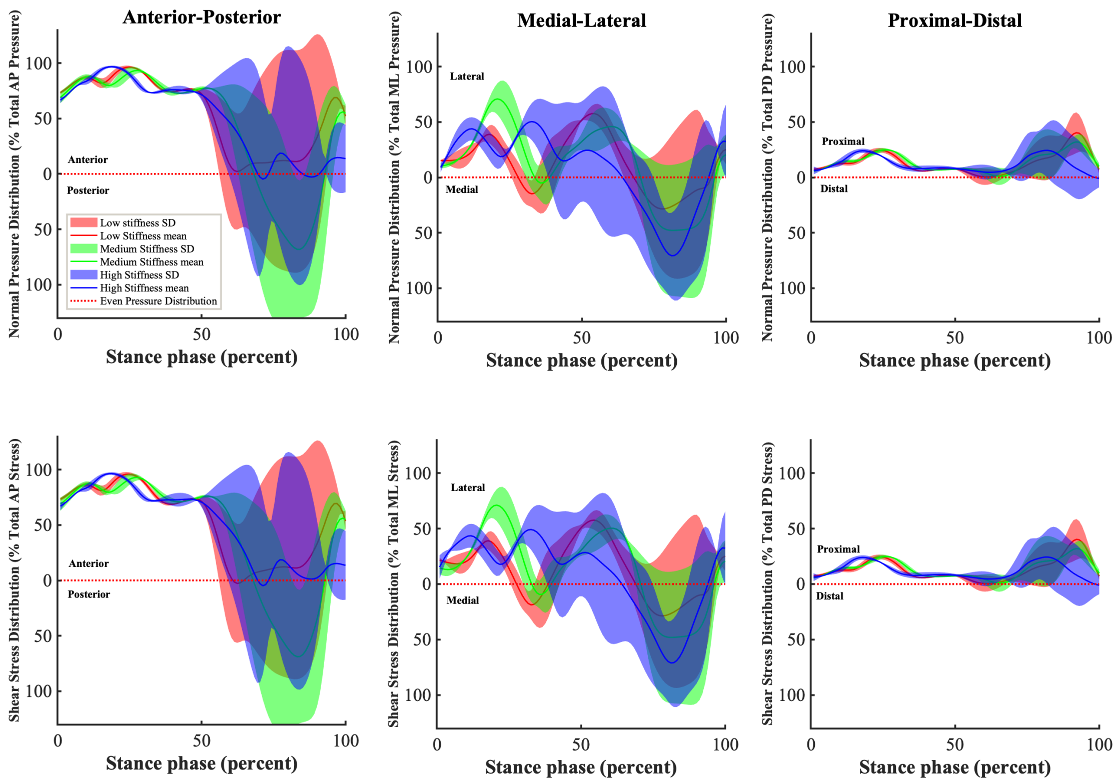

Figure 5: Subject 1 mean data for normal pressure (top) and shear stress (bottom) distributions in the anterior-posterior, medial-lateral, and proximal-distal directions.

Table 3: Average peak values for normal and shear stress (average of nine anatomical locations), and peak values for residual limb piston displacement with respect to the prosthetic socket. Data are mean ± SD.

Subject (condition)	Normal Pressure (kPa)	Shear Stress (kPa)	Piston Displacement (cm)
1 (low)	75.7 ± 3.71	26.8 ± 1.26	1.48 ± 0.02
1 (medium)	72.7 ± 6.42	25.5 ± 2.22	1.51 ± 0.01
1 (high)	81.54 ± 4.11	28.5 ± 1.44	1.50 ± 0.03
2 (low)	91.2 ± 10.93	32.0 ± 3.84	1.95 ± 0.10
2 (medium)	103 ± 6.47	36.1 ± 2.30	2.07 ± 0.15
2 (high)	119.2 ± 32.6	42.1 ± 11.7	2.09 ± 0.19
3 (low)	50.5 ± 1.08	18.6 ± 0.47	1.22 ± 0.01
3 (medium)	52.1 ± 0.61	18.2 ± 0.19	1.26 ± 0.02
3 (high)	61.0 ± 13.9	21.5 ± 4.89	1.26 ± 0.02
4 (low)	64.1 ± 1.41	22.5 ± 22.5	1.19 ± 0.00
4 (medium)	76.1 ± 4.24	36.6 ± 1.50	1.22 ± 0.03
4 (high)	78.3 ± 1.26	27.4 ± 0.42	1.19 ± 0.03
Group (low)	70.4 ± 4.28	25.0 ± 1.52	1.46 ± 0.03
Group (medium)	78.1 ± 4.44	26.6 ± 1.55	1.52 ± 0.05
Group (high)	85.0 ± 13.0	29.9 ± 4.61	1.51 ± 0.07

Table 4: Average peak values for normal pressure (kPa) by anatomical location, subject, and condition. A zero value for the distal contact interface implies that the distal tibia did not contact the base of the prosthetic socket (i.e. piston displacement < 1.5 cm). Data are mean ± SD.

Subject (condition)	Anterior Proximal	Anterior Distal	Posterior Proximal	Posterior Distal	Medial Proximal	Medial Distal	Lateral Proximal	Lateral Distal	Distal
1 (low)	259 ± 30.6	132 ± 6.52	41.5 ± 24.9	20.6 ± 4.86	72.9 ± 29.9	47.4 ± 1.61	84.1 ± 2.25	68.6 ± 3.28	0.08 ± 0.06
1 (medium)	238 ± 41.9	123 ± 12.0	53.4 ± 19.4	22.2 ± 4.23	78.1 ± 44.4	43.8 ± 7.41	128 ± 17.6	73.7 ± 4.35	4.91 ± 5.34
1 (high)	292 ± 14.2	141 ± 6.99	39.2 ± 15.2	20.9 ± 2.74	58.3 ± 15.9	40.0 ± 2.19	99.7 ± 10.4	73.3 ± 4.95	4.91 ± 5.34
2 (low)	199 ± 19.2	118 ± 13.9	34.5 ± 6.84	24.5 ± 0.95	56.0 ± 11.3	40.5 ± 2.72	275 ± 32.4	128 ± 11.9	89.5 ± 33.8
2 (medium)	358 ± 44.3	138 ± 12.3	29.9 ± 17.9	25.0 ± 1.03	49.9 ± 11.2	41.0 ± 3.13	283 ± 52.4	132 ± 23.3	145 ± 39.7
2 (high)	320 ± 21.4	196 ± 49.4	27.5 ± 3.37	36.6 ± 11.7	53.4 ± 15.7	71.7 ± 26.4	182 ± 31.8	131 ± 38.4	233 ± 104
3 (low)	131 ± 14.5	81.8 ± 4.62	80.1 ± 5.52	42.5 ± 3.11	76.5 ± 4.08	43.7 ± 3.01	111 ± 16.6	74.5 ± 7.04	0.00 ± 0.00
3 (medium)	151 ± 7.19	87.5 ± 2.46	57.7 ± 8.35	32.4 ± 3.90	69.4 ± 12.5	43.1 ± 5.46	90.1 ± 13.1	55.4 ± 3.07	0.00 ± 0.00
3 (high)	160 ± 3.20	87.7 ± 3.86	88.2 ± 51.4	45.7 ± 26.0	87.0 ± 13.3	54.1 ± 7.38	103 ± 23.6	75.7 ± 25.1	0.00 ± 0.00
4 (low)	188 ± 12.5	37.2 ± 5.50	17.1 ± 0.72	15.7 ± 0.72	38.1 ± 2.53	32.4 ± 2.02	138 ± 6.97	71.8 ± 2.53	0.00 ± 0.00
4 (medium)	256 ± 25.0	122 ± 9.51	26.1 ± 6.90	16.4 ± 0.57	43.3 ± 3.56	37.5 ± 0.39	145 ± 5.49	75.2 ± 1.53	0.00 ± 0.00
4 (high)	271 ± 0.24	128 ± 0.92	42.3 ± 2.83	17.8 ± 0.78	35.9 ± 4.11	30.3 ± 2.20	139 ± 7.78	73.6 ± 3.19	0.00 ± 0.00
Group (low)	194 ± 19.2	107 ± 7.65	43.3 ± 9.50	25.8 ± 2.41	60.7 ± 12.0	41.0 ± 2.34	152 ± 14.5	85.8 ± 6.19	22.4 ± 8.46
Group (medium)	251 ± 29.6	118 ± 9.05	41.8 ± 13.1	24.0 ± 2.44	60.2 ± 17.9	41.3 ± 4.10	162 ± 22.2	84.0 ± 8.05	36.9 ± 10.0
Group (high)	261 ± 9.77	138 ± 15.3	49.3 ± 18.2	30.3 ± 10.3	58.6 ± 12.3	49.0 ± 9.55	131 ± 18.4	88.5 ± 17.9	59.5 ± 27.4

Table 5: Average peak values for shear stress (kPa) by anatomical location, subject, and condition. A zero value for the distal contact interface implies that the distal tibia did not contact the base of the prosthetic socket (i.e. piston displacement < 1.5 cm). Data are mean ± SD.

Subject (condition)	**Anterior Proximal**	**Anterior Distal**	**Posterior Proximal**	**Posterior Distal**	**Medial Proximal**	**Medial Distal**	**Lateral Proximal**	**Lateral Distal**	**Distal**
1 (low)	90.5 ± 10.7	46.3 ± 2.33	15.4 ± 8.13	8.08 ± 2.10	26.9 ± 9.58	16.7 ± 0.76	29.7 ± 1.01	24.7 ± 1.14	0.03 ± 0.02
1 (medium)	83.1 ± 14.7	43.3 ± 4.17	19.0 ± 6.27	8.61 ± 1.78	27.9 ± 15.1	16.5 ± 3.47	44.7 ± 6.25	25.8 ± 1.61	0.98 ± 0.23
1 (high)	102 ± 4.98	49.5 ± 2.44	13.7 ± 5.35	7.51 ± 0.96	20.8 ± 5.05	14.1 ± 0.82	35.4 ± 3.97	26.1 ± 1.74	1.90 ± 1.99
2 (low)	69.9 ± 6.71	41.3 ± 4.89	12.1 ± 2.34	8.62 ± 0.35	19.6 ± 3.95	14.4 ± 1.23	96.5 ± 11.4	45.0 ± 4.32	35.8 ± 12.9
2 (medium)	127 ± 18.1	48.2 ± 4.30	10.5 ± 6.25	8.89 ± 0.23	17.5 ± 3.92	14.3 ± 1.10	99.3 ± 18.5	46.5 ± 8.35	51.7 ± 13.1
2 (high)	120 ± 10.2	68.9 ± 17.5	10.2 ± 1.90	12.9 ±4.18	19.4 ± 5.94	25.7 ± 9.65	64.7 ± 11.5	46.7 ± 13.9	81.9 ± 36.4
3 (low)	45.8 ± 5.10	28.6 ± 1.63	28.3 ± 1.97	15.4 ± 1.10	26.8 ± 1.43	15.3 ± 1.06	40.1 ± 5.32	27.3 ± 2.38	0.00 ± 0.00
3 (medium)	52.8 ± 2.51	30.6 ± 0.87	20.4 ± 2.91	11.6 ± 1.42	24.7 ± 4.76	15.5 ± 2.17	31.5 ± 4.58	19.5 ± 1.01	0.00 ± 0.00
3 (high)	55.9 ± 1.13	30.7 ± 1.34	31.0 ± 18.0	16.3 ± 8.99	30.4 ± 4.66	19.0 ± 2.69	36.3 ± 8.41	26.8 ± 8.95	0.00 ± 0.00
4 (low)	65.7 ± 4.37	34.0 ± 1.93	6.01 ± 0.27	5.54 ± 0.31	13.8 ± 0.69	12.2 ± 1.21	48.3 ± 2.43	25.1 ± 0.85	0.00 ± 0.00
4 (medium)	89.8 ± 8.74	42.8 ± 3.33	9.11 ± 2.42	5.73 ± 0.19	15.3 ± 1.37	13.5 ± 0.38	50.9 ± 1.93	16.3 ± 0.54	0.00 ± 0.00
4 (high)	95.0 ± 0.08	44.9 ± 0.32	15.9 ± 0.08	6.71 ± 0.73	13.7 ± 2.53	11.0 ± 0.37	48.5 ± 2.71	25.8 ± 1.16	0.00 ± 0.00
Group (low)	68.0 ± 6.72	37.6 ± 2.70	15.4 ± 3.18	9.41 ± 0.97	21.8 ± 3.91	14.7 ± 1.06	53.7 ± 5.03	30.5 ± 2.17	8.95 ± 3.23
Group (medium)	88.2 ± 11.0	41.2 ± 3.17	14.7 ± 4.46	8.70 ± 0.91	21.4 ± 6.28	14.9 ± 1.78	56.6 ± 7.82	29.5 ± 2.88	13.2 ± 3.33
Group (high)	93.3 ± 4.09	48.5 ± 5.40	17.7 ± 6.33	10.9 ± 3.72	21.1 ± 4.54	17.5 ± 3.38	46.2 ± 6.59	31.3 ± 6.43	21.0 ± 9.58

4.0 Discussion

4.1 Model Performance (Group Data)

The objective of this study was to develop a spatial contact model of the residual limb-prosthetic socket interface and evaluate its ability to estimate limb-socket interface dynamics. A secondary objective of this study was to use this model to examine the relationships between prosthetic foot stiffness and limb-socket dynamics. Model-derived values for normal pressure depict spatiotemporal patterns similar to those of a ground reaction force (GRF) curve during stance phase. The pressure and shear waveforms presented by Sanders et al. (1992) and Laszczak et al. (2016) are similar to those of the present study early in stance phase, but exhibit a brief plateau during mid-stance before values decrease. Comparatively, the present study shows similar loading rates, but a gradual decline in pressure and stress rather than a mid-stance phase plateau (i.e. the waveforms are skewed toward early stance phase) (Figure 2). The lack of a plateau in pressure and shear data in the present results may be due to inadequate constraining of residual limb motion. Using experimental kinematic data to constrain residual limb motion may help refine the trajectory of the modeled response. Alternatively, a velocity constraint could be implemented into the present model design.

Peak values for normal pressure were similar to those reported in previous sensor-based experiments (Courtney et al., 2016; Laszczak et al., 2016; J. E. Sanders et al., 1992; J E Sanders et al., 2000) and finite element modeling-based analyses (Jia et al., 2004; Lee et al., 2004; Portnoy et al., 2009), which ranged from 40-160 kPa. Similarly, values for shear stress were within the 3-50 kPa range reported previously (Laszczak et al., 2016; Noll et al., 2017; Sanders and Daly, 1993; Schiff et al., 2014).

The ability of the model to predict pressure and shear stress values specific to different anatomical locations is difficult to discern based on previous experiments. Previous sensor-based experiments have typically sampled from small localized areas on the limb or present only resultant data. Nevertheless, broad comparisons can be made with data from Sanders et al. (1992), Sanders et al. (2000), and Courtney et al. (2016). Results of this study showed peak mean pressure and stress values on the medial side of approximately 60 and 21 kPa (values are the mean of the proximal and distal interfaces under all stiffness conditions). Data from Courtney et al. (2016) showed peak medial pressure to be approximately 65-70 kPa, whereas Sanders et al. (2000) present values ranging from 40-85 kPa for pressure and 7-12 kPa for shear stress. On the lateral side, results of this study showed peak mean pressure and shear stress values of approximately 117 and 41 kPa. Comparatively, Sanders et al. (2000) present values of 60-140 kPa for pressure and 18-23 kPa for shear stress. Posteriorly, the pressure and shear values of 41 and 13 kPa were lower compared to those presented by Sanders et al. (85-100 and 17-22 kPa). This discrepancy may be due to the increased stiffness of the tissue on the posterior residual limb associated with muscle contraction during gait, which is unaccounted for in this model. Muscular contraction has been shown to increase tissue modulus by 45 kPa (Zheng et al., 1999). Muscular contraction would likely have minimal effects on the frictional characteristics of the tissue. In the future, a progressive model of tissue moduli could be implemented into limb-socket contact model. The model's predicted anterior pressure and shear stress were 235 and 83 kPa, which were similar to values of 245 and 105 derived from FEA of socket interface dynamics at the patellar tendon (Lee et al., 2004). There is a paucity of data from sensor-based experiments related to pressure or shear dynamics along the tibial plateau.

The model predicted peak residual limb displacements between 1.2 and 2.1 cm with respect to the socket. These values are within the range of 1.1-3.6 cm (mean: 2.3 ± 1.0 cm) previously reported in the literature (Gholizadeh et al., 2011; Grevsten & Erikson, 1975; LaPrè et al., 2018; Narita, Yokogushi, Shii, Kakizawa, & Nosaka, 1997; Joan E. Sanders et al., 2006; Söderberg, Ryd, & Persson, 2003; Wirta et al., 1990). It should be noted that the prosthetic socket components (e.g. liner and socket materials) and gait tasks varied between these studies. Data from the present study, among others support the idea that the amount of residual limb pistoning may be affected by liner and socket type (J E Sanders et al., 2000; Yiğiter, Şener, & Bayar, 2002), residual limb shape (Wirta et al., 1990), and gait conditions (Gholizadeh et al., 2011; J E Sanders et al., 2000). Data regarding the prosthetic socket componentry used by participants in this study were not available.

The pressure distribution profiles derived from this model were weighted toward the anterior and lateral aspects of the residual limb. These patterns may be due in part to gait kinematics of the participants. However, this may also be a result of the modulus values used to parameterize the contact interfaces. These values were 3.5 times higher for the anterior aspect of the tibia compared to posterior, and 1.4 times higher for the lateral compared to medial aspects. Increasing the number of contact points in the model may lead to a higher resolution representation of the material properties of the residual limb as they vary by anatomical location. However, this would likely increase computation time.

4.2 Computation Time

Computation time is an important consideration in simulation-based analytical approaches. Compared to previous simulations using this gait model, the addition of the residual limb-socket spatial contact model resulted in 34.5%, 28.9%, and 25.5% increases in execution times for the low, medium, and high stiffness conditions, respectively. These values correspond to increases of 20.2, 17.1, and 58.6 s. Increased execution times may be attributed increased model complexity, but also potentially to a suboptimal ratio of stiffness:damping within the limb-socket contact model. These conditions can result in small oscillations within the model's force signals, causing the solver to reduce the step sizes used for numerical integration. Optimization of the stiffness:damping ratio may improve execution times.

4.3 Case Study (Subject 1)

This study represents the first systematic evaluation of the effects of prosthetic foot stiffness on residual limb-prosthetic socket interface dynamics. Across the stiffness conditions, outcome measures for Subject 1 showed similar spatiotemporal patterns between 0-50% stance phase (Figure 4), which encompass progression from heel strike to foot flat (Winter, 1991). Divergent responses were observed across the stiffness conditions in the latter half of stance phase for residual limb axial angle and anterior-posterior pressure and shear stress distribution. Increased variability was also observed for all conditions during this time. The latter half of stance phase may be characterized by the progression from foot flat to toe off and involves an anterior shift in the center of pressure (CoP) (Winter, 1991). Since the stiffness behavior of the VSF's heel is unchanged across the conditions, it is logical that the effects of variable forefoot stiffness would be primarily observed in the latter half of stance phase.

The subject presented no discernable effect of variable stiffness on peak average normal pressure, shear stress, or piston motion (Figure 4). Decreased external rotation was observed in the low stiffness condition, although high variability was present in the high stiffness condition. Increased external rotation may direct knee loading out of the sagittal plane and into the frontal plane, thereby compromising the ability of the knee to absorb forces and causing overloading of cartilage (Gailey, Allen, Castles, Kucharik, & Roeder, 2008). Increased external rotation has been also associated with high rates of medial knee osteoarthritis (Weidow, Tranberg, Saari, & Kärrholm, 2006). Elevated rates of knee osteoarthritis have been documented for both the amputated and contralateral limb for lower limb prosthesis users (Gailey et al., 2008).

There were no discernable effects of prosthesis stiffness on frontal or coronal plane pressure or shear stress distribution. This response is consistent with the mechanical principles of the VSF, which modulates forefoot stiffness primarily in the sagittal plane. From 0-50% stance phase, the subject exhibited a more anteriorly-directed distribution, which transitioned to a relatively even anterior-posterior distribution in the latter half of stance phase for the low and high stiffness conditions. In the medium stiffness condition, pressure and shear stress were more posteriorly-directed. High variability was observed across the three trials per condition, and therefore more data are necessary to determine the consistency of these patterns.

4.4 Limitations and Future Directions

The present model was parameterized using previously reported residual limb tissue mechanical properties and limb-socket kinematics for individuals with BKA. While these methods resulted in pressure and shear stress values within the range reported in the literature, the variability in the aforementioned parameters is well documented between individual subjects. Future work should strive toward individualized models by characterizing the tissue mechanical properties of subjects. Similarly, adjusting parameters based on the socket componentry used by subjects would improve the accuracy of the model. For example, coefficients of friction between 0.5-3.0 have been reported for the interaction between human skin and various socket liner materials (Cagle et al., 2018; Joan E Sanders et al., 1998). Variation within this range would have a substantial impact on model-derived shear force estimates.

Future work should also seek to quantify kinematics between the residual limb and prosthetic socket through optical motion capture or instrumenting participants with potentiometers. Using these data to constrain residual limb motion during simulations would improve accuracy on an individualized basis. Further, these data could be used to refine the ability of the current model to predict limb-socket kinematics.

The present model assumes oversimplified geometries of the residual limb and prosthetic socket. Developing more complex interface geometry could improve the fidelity of the model. For example, using a pentagonal prism shape to model the residual limb geometry would allow for differentiation of the varying moduli of the anterior, anterior lateral, anterior medial, posterior lateral, and posterior medial aspects of the residual limb and would only add two interface frames compared to the present model.

This study modeled the residual limb as composite of both the bone and soft tissue elements. However, data from x-ray (Lilja, Johansson, & Öberg, 1993) and biplane fluoroscopy (Bocobo, Castellote, MacKinnon, & Gabrielle-Bergman, 1998) studies suggest that residual limb kinematics can be differentiated into the motion of the bone and soft tissue elements. As such, it may be important to distinguish these elements and model the interface between them in future studies. Doing so could lead to improvements when simulating limb-socket dynamics.

5.0 Conclusions

Data from this study support the use of reduced order modeling techniques to estimate residual limb-prosthetic socket interfacial pressure and shear stress, as well as residual limb kinematics in a computationally economical manner. Limitations include parameterization of the contact models based on data previously reported in the literature, rather than data measured from subjects in this study. Nevertheless, residual limb-prosthetic socket interface dynamics derived from this model were within the range of values reported by previous sensor-based gait experiments. These methods may be useful to aid experimental studies by providing insights into the effects of varied prosthesis design parameters or gait conditions on residual limb-socket interface dynamics.

Data from a case study show promise for evaluating the effects of prosthesis stiffness on limb-socket dynamics. Variable prosthesis stiffness did not appear to affect residual limb pistoning, nor peak normal pressure or shear stress. The low stiffness condition resulted in decreased external rotation compared to the medium and high stiffness conditions. However, data displayed high variability and further investigation is necessary to discern the repeatability of this effect. Future work could add complexity to the modeled interface geometry in order to better match the shape and variation in tissue material properties of the residual limb. Additionally, the model's accuracy could be improved by applying subject-specific data for residual limb tissue properties and prosthetic socket componentry when parameterizing the contact interfaces.

Acronyms widely used in text

AP	Anterior-Posterior
BKA	Below-Knee Amputation
DoF	Degrees of Freedom
LLA	Lower Limb Amputation
ML	Medial-Lateral
Ode23t	Ordinary Differential Equation 23 trapezoidal solver
PD	Proximal-Distal
SD	Standard Deviation
VSF	Variable Stiffness Foot

Abbreviations

F	Force, N
k	Linear stiffness, N/mm
μ	Coefficient of friction
v	Linear velocity
δ	Penetration depth, mm
$\dot{\delta}$	Penetration velocity, mm/s

Superscripts and subscripts

F_f	Frictional force, N
F_n	Normal force, N
v_{poc}	Linear velocity at point of contact, mm/s
$v_{\mathrm{threshold}}$	Linear velocity threshold, m/s
μ_{kinetic}	Coefficient of kinetic friction
μ_{static}	Coefficient of static friction

References

Al-Fakih, E. A., Osman, N. A. A., Eshraghi, A., & Adikan, F. R. M. (2013). The capability of fiber Bragg grating sensors to measure amputees' trans-tibial stump/socket interface pressures. *Sensors (Switzerland)*, *13*(8), 10348–10357. https://doi.org/10.3390/s130810348

Ali, S., Abu Osman, N. A., Eshraghi, A., Gholizadeh, H., Abd Razak, N. A. Bin, & Wan Abas, W. A. B. Bin. (2013). Interface pressure in transtibial socket during ascent and descent on stairs and its effect on patient satisfaction. *Clinical Biomechanics*, *28*(9–10), 994–999. https://doi.org/10.1016/j.clinbiomech.2013.09.004

Balk, E. M., Gazula, A., Markozannes, G., Kimmel, H. J., Saldanha, I. J., Resnik, L. J., & Trikalinos, T. A. (2018). *Lower Limb Prostheses: Measurement Instruments, Comparison of Component Effects by Subgroups, and Long-Term Outcomes*. https://doi.org/10.23970/AHRQEPCCER213

Bocobo, C., Castellote, J., MacKinnon, D., & Gabrielle-Bergman, A. (1998). Videofluoroscopic evaluation of prosthetic fit and residual limbs following transtibial amputation. *Journal of Rehabilitation Research and Developmenth*, *35*(1), 6–13.

Boutwell, E., Stine, R., Hansen, A., Tucker, K., & Gard, S. (2012). Effect of prosthetic gel liner thickness on gait biomechanics and pressure distribution within the transtibial socket. *Journal of Rehabilitation Research and Development*, *49*(2), 227–240. https://doi.org/10.1682/JRRD.2010.06.0121

Cagle, J. C., Hafner, B. J., Taflin, N., & Sanders, J. E. (2018). Characterization of prosthetic liner products for people with transtibial amputation. *Journal of Prosthetics and Orthotics*, *30*(4), 187–199. https://doi.org/10.1097/JPO.0000000000000205

Courtney, A., Orendurff, M. S., & Buis, A. (2016). Effect of alignment perturbations in a trans-tibial prosthesis user: A pilot study. *Journal of Rehabilitation Medicine*, *48*(4), 396–401. https://doi.org/10.2340/16501977-2075

Darter, B. J., Sinitski, K., & Wilken, J. M. (2016). Axial bone-socket displacement for persons with a traumatic transtibial amputation: The effect of elevated vacuum suspension at progressive body-weight loads. *Prosthetics and Orthotics International*, *40*(5), 552–557. https://doi.org/10.1177/0309364615605372

De Leva, P. (1996). Adjustments to zatsiorsky-seluyanov's segment inertia parameters. *Journal of Biomechanics*, *29*(9), 1223–1230. https://doi.org/10.1016/0021-9290(95)00178-6

Eshraghi, A., Osman, N. A. A., Gholizadeh, H., Karimi, M., & Ali, S. (2012). Pistoning assessment in lower limb prosthetic sockets. *Prosthetics and Orthotics International*, *36*(1), 15–24. https://doi.org/10.1177/0309364611431625

Gailey, R., Allen, K., Castles, J., Kucharik, J., & Roeder, M. (2008). Review of secondary physical conditions associated with lower-limb amputation and long-term prosthesis use. *JRRD*, *45*(1), 15–30. https://doi.org/10.1682/JRRD.2006.11.0147

Gholizadeh, H., Azuan, N., Osman, A., Eshraghi, A., Anuar, N., & Razak, A. (2014). Clinical implication of interface pressure for a new prosthetic suspension system. *BioMedical Engineering OnLine*, *13*(89). https://doi.org/10.1186/1475-925X-13-89

Gholizadeh, H., Osman, N. A. A., Lúvíksdóttir, Á. G., Eshraghi, A., Kamyab, M., & Wan Abas, W. A. B. (2011). A new approach for the pistoning measurement in transtibial prosthesis. *Prosthetics and Orthotics International*, *35*(4), 360–364. https://doi.org/10.1177/0309364611423130

Grevsten, S., & Erikson, U. (1975). A roentgenological study of the stump-socket contact and skeletal displacement in the PTB-suction prosthesis. *Upsala Journal of Medical Sciences*, *80*(1), 49–57. https://doi.org/10.3109/03009737509178991

Henrikson, K. M., Weathersby, E. J., Larsen, B. G., Cagle, J. C., McLean, J. B., & Sanders, J. E. (2018). An inductive sensing system to measure in-socket residual limb displacements for people using lower-limb prostheses. *Sensors*, *18*(11). https://doi.org/10.3390/s18113840

Highsmith, J. T., & Highsmith, M. J. (2007). Common skin pathology in LE prosthesis users. *Journal of the American Academy of Physician Assistants*, *20*(11), 33–36. https://doi.org/10.1097/01720610-200711000-00018

Highsmith, M. J., Kahle, J. T., Klenow, T. D., Andrews, C. R., Lewis, K. L., Bradley, R. C., … Highsmith, J. T. (2016). Interventions to manage residual limb ulceration due to prosthetic use in individuals with lower extremity amputaiton: A systematic review of the literature, *18*(3), 115–123. https://doi.org/10.21300/18.2-3.2016.115

Jia, X., Zhang, M., & Lee, W. C. C. (2004). Load transfer mechanics between trans-tibial prosthetic socket and residual limb - Dynamic effects. *Journal of Biomechanics*, *37*, 1371–1377. https://doi.org/10.1016/j.jbiomech.2003.12.024

LaPrè, A. K., Price, M. A., Wedge, R. D., Umberger, B. R., & Sup, F. C. (2018). Approach for gait analysis in persons with limb loss including residuum and prosthesis socket dynamics. *International Journal for*

Numerical Methods in Biomedical Engineering, *34*(4), e2936. https://doi.org/10.1002/cnm.2936

Laprè, A. K., Umberger, B. R., & Sup, F. (2014). Simulation of a powered ankle prosthesis with dynamic joint alignment. In *2014 36th Annual International Conference of the IEEE Engineering in Medicine and Biology Society, EMBC 2014*. https://doi.org/10.1109/EMBC.2014.6943914

Laszczak, P., Jiang, L., Bader, D. L., Moser, D., & Zahedi, S. (2015). Development and validation of a 3D-printed interfacial stress sensor for prosthetic applications. *Medical Engineering and Physics*, *37*(1), 132–137. https://doi.org/10.1016/j.medengphy.2014.10.002

Laszczak, P., Mcgrath, M., Tang, J., Gao, J., Jiang, L., Bader, D. L., … Zahedi, S. (2016). A pressure and shear sensor system for stress measurement at lower limb residuum/socket interface. *Medical Engineering and Physics*, *38*, 695–700. https://doi.org/10.1016/j.medengphy.2016.04.007

Lee, W. C. C., Zhang, M., Jia, X., & Cheung, J. T. M. (2004). Finite element modeling of the contact interface between trans-tibial residual limb and prosthetic socket. *Medical Engineering & Physics*, *26*, 655–662. https://doi.org/10.1016/j.medengphy.2004.04.010

Lilja, M., Johansson, T., & Öberg, T. (1993). Movement of the tibial end in a PTB prosthesis socket: A sagittal X-ray study of the PTB prosthesis. *Prosthetics and Orthotics International*, *17*(1), 21–26. https://doi.org/10.3109/03093649309164351

Mak, A. F. T., George, ;, Liu, H. W., & Lee, ; S Y. (1994). Biomechanical assessment of below-knee residual limb tissue. *Journal of Rehabilitation Research and Development*, *31*(3), 188–198.

Meulenbelt, H. E. J., Dijkstra, P. U., Jonkman, M. F., & Geertzen, J. H. B. (2006, May). Skin problems in lower limb amputees: A systematic review. *Disability and Rehabilitation*. Taylor & Francis. https://doi.org/10.1080/09638280500277032

Narita, H., Yokogushi, K., Shii, S., Kakizawa, M., & Nosaka, T. (1997). Suspension effect and dynamic evaluation of the total surface bearing (TSB) trans-tibial prosthesis: A comparison with the patellar tendon bearing (PTB) trans-tibial prosthesis. *Prosthetics and Orthotics International*, *21*(3), 175–178. https://doi.org/10.3109/03093649709164551

National Health Services Audit Commission Briefing: Assisting Independence. (2002).

Noll, V., Eschner, N., Schumacher, C., Beckerle, P., & Rinderknecht, S. (2017). A physically-motivated model describing the dynamic interactions between residual limb and socket in lower limb prostheses. *Current Directions in Biomedical Engineering*, *3*(1), 15–18. https://doi.org/10.1515/cdbme-2017-0004

Portnoy, S., Siev-Ner, I., Shabshin, N., Kristal, A., Yizhar, Z., & Gefen, A. (2009). Patient-specific analyses of deep tissue loads post transtibial amputation in residual limbs of multiple prosthetic users. *Journal of Biomechanics*, *42*, 2686–2693. https://doi.org/10.1016/j.jbiomech.2009.08.019

Safari, M. R., Tafti, N., & Aminian, G. (2015). Socket Interface Pressure and Amputee Reported Outcomes for Comfortable and Uncomfortable Conditions of Patellar Tendon Bearing Socket: A Pilot Study. *Assistive Technology*, *27*(1), 24–31. https://doi.org/10.1080/10400435.2014.949016

Sanders, J. E., Daly, C. H., & Burgess, E. M. (1992). Interface shear stresses during ambulation with a below-knee prosthetic limb. *Journal of Rehabilitation Research and Development*, *29*(4), 1–8. https://doi.org/10.1682/jrrd.1992.10.0001

Sanders, J E, Zachariah, S. G., Baker, A. B., Greve, J. M., & Clinton, C. (2000). Effects of changes in cadence, prosthetic componentry, and time on interface pressures and shear stresses of three trans-tibial amputees. *Clinical Biomechanics*, *15*, 684–694. Retrieved from www.elsevier.com/locate/clinbiomech

Sanders, Joan E., & Daly, C. H. (1993). Measurement of Stresses in Three Orthogonal Directions at the Residual Limb-Prosthetic Socket Interface. *IEEE Transactions on Rehabilitation Engineering*, *1*(2), 79–85. https://doi.org/10.1109/86.242421

Sanders, Joan E., Karchin, A., Fergason, J. R., & Sorenson, E. A. (2006). A noncontact sensor for measurement of distal residual-limb position during walking. *Journal of Rehabilitation Research and Development*, *43*(4), 509–516. https://doi.org/10.1682/JRRD.2004.11.0143

Sanders, Joan E, Greve, J. M., Mitchell, S. B., & Zachariah, S. G. (1998). Material properties of commonly-used interface materials and their static coefficients of friction with skin and socks. *Journal of Rehabilitation Research and Development*, *35*(2), 161–176.

Schiff, A., Havey, R., Carandang, G., Wickman, A., Angelico, J., Patwardhan, A., & Pinzur, M. (2014). Quantification of Shear Stresses Within a Transtibial Prosthetic Socket. *Foot & Ankle International*, *35*(8), 779–782. https://doi.org/10.1177/1071100714535201

Shan, X., Otsuka, S., Yakura, T., Naito, M., Nakano, T., & Kawakami, Y. (2019). Morphological and mechanical properties of the human triceps surae aponeuroses taken from elderly cadavers: Implications for muscle-tendon interactions. *PLoS ONE*, *14*(2). https://doi.org/10.1371/journal.pone.0211485

Söderberg, B., Ryd, L., & Persson, B. M. (2003). Roentgen Stereophotogrammetric Analysis of Motion between the Bone and the Socket in a Transtibial Amputation Prosthesis: A Case Study. *Journal of Prosthetics and Orthotics*, *15*(3), 95–99. https://doi.org/10.1097/00008526-200307000-00008

Weidow, J., Tranberg, R., Saari, T., & Kärrholm, J. (2006). Hip and Knee Joint Rotations Differ between Patients with Medial and Lateral Knee Osteoarthritis: Gait Analysis of 30 Patients and 15 Controls. *J Orthop Res*, *24*, 1890–1899. https://doi.org/10.1002/jor.20194

Winter, D. A. (1991). *The Biomechanics and Motor Control of Human Gait*.

Wirta, R. W., Golbranson, F. L., Mason, R., & Calvo, K. (1990). Analysis of below-knee suspension systems : Effect on gait. *Journal of Rehabilitation Research and Development*, *27*(4), 385–396. https://doi.org/10.1682/JRRD.1990.10.0385

Yiğiter, K., Şener, G., & Bayar, K. (2002). Comparison of the effects of patellar tendon bearing and total surface bearing sockets on prosthetic fitting and rehabilitation. *Prosthetics and Orthotics International*, *26*(3), 206–212. https://doi.org/10.1080/03093640208726649

Zheng, Y., Mak, A. F. T., & Lue, B. (1999). Objective assessment of limb tissue elasticity: Development of a manual indentation procedure. *Journal of Rehabilitation Research and Development*, *36*(2), 71–85.